Acta Crystallographica Section D
**Biological Crystallography**
ISSN 0907-4449

# Structure of the human filamin A actin-binding domain

**Salla Ruskamo* and Jari Ylänne**

The Department of Biological and Environmental Science, PO Box 35, University of Jyväskylä, FIN-40014 Jyväskylä, Finland

Correspondence e-mail: salla.ruskamo@jyu.fi

Received 24 June 2009
Accepted 15 September 2009

**PDB Reference:** human filamin A actin-binding domain, 2wfn, r2wfnsf.

Filamin A (FLNa) is a large dimeric protein that binds to actin filaments *via* its actin-binding domain (ABD). The crystal structure of this domain was solved at 3.2 Å resolution. The domain adopts a closed conformation typical of other ABDs, but also forms a dimer both in crystallization conditions and in solution. The structure shows the localization of the residues mutated in patients with periventricular nodular heterotopia or otopalatodigital syndrome. Structural analysis predicts that mutations in both types of disorder may affect actin binding.

## 1. Introduction

Filamins (FLNs) are large actin cross-linkers that also participate in the regulation of cell movement and cell signalling. Human FLNs are homodimers of 280 kDa polypeptides that contain an N-terminal actin-binding domain (ABD) and 24 immunoglobulin-like domains (Feng & Walsh, 2004; van der Flier & Sonnenberg, 2001). The ABDs of FLNs contain two calponin-homology (CH) domains and are similar to the ABDs of spectrins, dystrophin, utrophin, $\alpha$-actinins, fibrins and plectins (Gimona *et al.*, 2002). Several genetic diseases that cause abnormalities in brain, bone and cardiovascular system development have been linked to mutations in the FLNa and FLNb genes. Some of the identified patient mutations causing otopalatodigital syndrome (OPD) spectrum disorders or periventricular nodular heterotopia (PVNH) have been mapped in the ABD of FLNa (Parrini *et al.*, 2006; Robertson, 2007). In this report, we describe the crystal structure of the ABD of FLNa. The 3.2 Å resolution structure reveals the predicted folding pattern consisting of two CH domains. Based on the FLNa ABD structure, we have mapped the exact locations of OPD and PVNH patient mutation residues in ABD and obtained more information about the defects caused by these mutations.

## 2. Materials and methods

### 2.1. Cloning, protein expression and purification

Human FLNa (accession code X53416) ABD containing residues 1–278 was generated by polymerase chain reaction and inserted into a modified pGEX vector (GE Healthcare, Chalfont St Giles, England) containing a tobacco etch virus (TEV) protease cleavage site. The insert was verified by sequencing. The glutathione-*S*-transferase (GST) fusion protein was expressed in LB medium containing 100 $\mu$g ml$^{-1}$

ampicillin and 0.4 m*M* isopropyl β-D-1-thiogalactopyranoside (IPTG) in *Escherichia coli* BL21 Gold (Stratagene, La Jolla, California, USA) at 310 K for 4 h starting at an $OD_{600}$ of 0.6. Cells were harvested by centrifugation, suspended in phosphate-buffered saline (PBS; 137 m*M* NaCl, 2 m*M* $KH_2PO_4$, 8 m*M* $Na_2HPO_4.2H_2O$, 3 m*M* KCl pH 7.4) and lysed by sonication. The lysate was centrifuged at 48 000*g* and 277 K for 30 min. GST-ABD was purified on Glutathione Sepharose 4B Fast Flow (GE Healthcare) according to the manufacturer's instructions. The N-terminal GST tag was cleaved by TEV protease at 277 K for 16 h, leaving a remnant Gly-Ala-Met-Gly peptide sequence. The solution was then desalted in 150 m*M* NaCl, 50 m*M* Tris–HCl pH 8.0 on a HiPrep 26/10 Desalting column (GE Healthcare) and the GST was removed from the solution using Glutathione Sepharose. The protein solution was gel-filtrated in 20 m*M* Tris–HCl pH 8.0 using a HiLoad 26/60 Superdex 75 prep-grade column (GE Healthcare) and finally concentrated using a Centriprep YM-10 (Millipore, Billerica, Massachusetts, USA). The composition of the protein solution used in crystallization trials was 20 mg ml$^{-1}$ in 20 m*M* Tris–HCl pH 8.0. Size-exclusion chromatography was performed in 20 m*M* Tris–HCl pH 8.0 using a Superdex 75 HR 10/30 column (GE Healthcare) and gel-filtration standards (BioRad Laboratories, Hercules, California, USA) were used to specify molecular weight.

### 2.2. Crystallization and data collection

Crystallization of the FLNa ABD was performed at 298 K using the hanging-drop vapour-diffusion technique with a 20 mg ml$^{-1}$ protein concentration. The FLNa ABD formed needle-like crystals of dimensions 0.05 × 0.05 × 1.5 mm in 2 µl droplets containing equal volumes of protein solution and reservoir solution (1.7 *M* lithium sulfate, 0.1 *M* HEPES pH 7.5) and was equilibrated against 1 ml reservoir solution. Crystals were frozen in liquid nitrogen in 25% glycerol, 1.5 *M* lithium sulfate and 0.1 *M* HEPES pH 7.5. Diffraction data were collected at 100 K on beamline ID14-2 at the European Synchrotron Radiation Facility and were processed using the *XDS* program package (Kabsch, 1993). The FLNa ABD crystals belonged to space group $C222_1$ in the orthorhombic crystal system. The unit-cell parameters were $a$ = 111.5, $b$ = 125.9, $c$ = 128.9 Å. There were two ABD molecules in the asymmetric unit, giving a Matthews coefficient of 3.6 Å$^3$ Da$^{-1}$ (Matthews, 1968) and a solvent content of 66%.

### 2.3. Structure determination and refinement

The crystal structure of FLNa ABD was solved by molecular replacement with *Phaser* (Storoni *et al.*, 2004) using the structure of α-actinin 1 ABD (PDB code 2eyi; Borrego-Diaz *et al.*, 2006) as the search model. Model building was then carried out manually using the program *Coot* (Emsley & Cowtan, 2004). The structure was further refined using *REFMAC* 5.5 (Murshudov *et al.*, 1997). Tight main-chain and side-chain noncrystallographic symmetry restraints between two ABD molecules in the asymmetric unit were used in the refinement. The geometry was also restrained tightly by applying an X-ray matrix-weighting term of 0.005 and the weight for the *B*-factor restraints was set to 0.5. The optimum matrix-weighting term was determined using the method described by Tickle (2007). The final $R_{cryst}$ and $R_{free}$ values of the model were 22.6% and 24.3%, respectively. The data-collection, structure-determination and refinement statistics are summarized in Table 1. All figures were generated and root-mean-square (r.m.s.) deviations of superimposed structures were calculated using *PyMOL* (DeLano Scientific, San Carlos, California, USA). The interaction surface of CH1 and CH2 was analyzed using the *PROTORP* server (http://www.bioinformatics.sussex.ac.uk/protorp).

**Table 1**
Data-collection, structure-determination and refinement statistics.

Values in parentheses are for the last resolution shell.

| | |
|---|---|
| Data collection | |
| Beamline | ESRF ID14-2 |
| Wavelength (Å) | 0.933 |
| Detector | ADSC CCD |
| Space group | $C222_1$ |
| Unit-cell parameters (Å) | $a$ = 111.5, $b$ = 125.9, $c$ = 128.9 |
| Matthews coefficient $V_M$ (Å$^3$ Da$^{-1}$) | 3.6 |
| Solvent content (%) | 66 |
| Resolution range (Å) | 42.20–3.20 (3.28–3.20) |
| $R_{merge}$† (%) | 11.9 (36.5) |
| Mean $I/\sigma(I)$ | 13.3 (3.99) |
| Completeness (%) | 99.6 (100.0) |
| Redundancy | 4.9 (20.2) |
| Refinement | |
| No. of unique reflections | 15280 |
| Refinement | 14518 (1055) |
| Test set | 764 (55) |
| No. of observed reflections | 72101 |
| $R_{work}/R_{free}$ (%) | 22.6/24.3 (33.3/29.8) |
| Correlation coefficients ($F_o - F_c/F_o - F_c$ free) | 0.876/0.860 |
| No. of atoms | 3696 |
| Protein | 3655 |
| Heterogen | 35 |
| Solvent | 6 |
| R.m.s. differences | |
| Bond lengths (Å) | 0.006 |
| Bond angles (°) | 1.014 |
| Isotropic $B$ factors (Å$^2$) | |
| Main chain | 38.7 |
| Side chain | 39.5 |
| Average $B$ factor excluding solvent (Å$^2$) | 39.1 |
| Amino acids in Ramachandran diagram (%) | |
| In most favoured regions | 88.2 |
| In additional allowed regions | 11.3 |
| In generously allowed regions | 0.5 |

† $R_{merge} = \sum_{hkl}\sum_i |I_i(hkl) - \langle I(hkl)\rangle| / \sum_{hkl}\sum_i I_i(hkl)$, where $I_i(hkl)$ is the intensity of the $i$th observation of unique reflection $hkl$.

## 3. Results and discussion

### 3.1. Overall structure

We determined the crystal structure of human FLNa ABD to 3.2 Å resolution. Because of poor or missing electron density, the N-terminal residues 1–40 and residues 155–165 in the linker region between the two CH domains were not built in the final model. The structure reveals the predicted folding pattern, in which two typical CH domains consist of four

dominant (*A*, *C*, *E* and *G*) and two short (*B* and *F*) helices. The CH domains lie near each other, forming a compact ABD (Fig. 1*b*). The interaction surface between the two CH domains is 800 Å$^2$. The two ABD molecules in the asymmetric unit are located antiparallel to each other, enabling contacts between CH1 of molecule *A* and CH2 of molecule *B* and *vice versa* (Fig. 1*a*). The interaction surface between the two molecules is 1247 Å$^2$ (10.8% of the total accessible surface of the molecules) and is composed of 42% polar atoms (11 hydrogen bonds and 15 salt bridges). These features indicate that the interface is rather tight, which is consistent with our finding from size-exclusion chromatography, based on the protein standards, that the recombinant proteins behaved mainly as a dimer.

### 3.2. Comparison with other ABDs and ABSs

The structure of FLNa ABD is highly similar to the structure of FLNb ABD (PDB code 3fer; A. P. Kuzin, M. Abashidze, R. Seetharaman, R. Shastry, S. Sahdev, C. Ciccosanti, R. Xiao, J. K. Everett, Y. Huang, T. Acton, B. Rost, G. T. Montelione, L. Tong & J. F. Hunt, unpublished work), giving

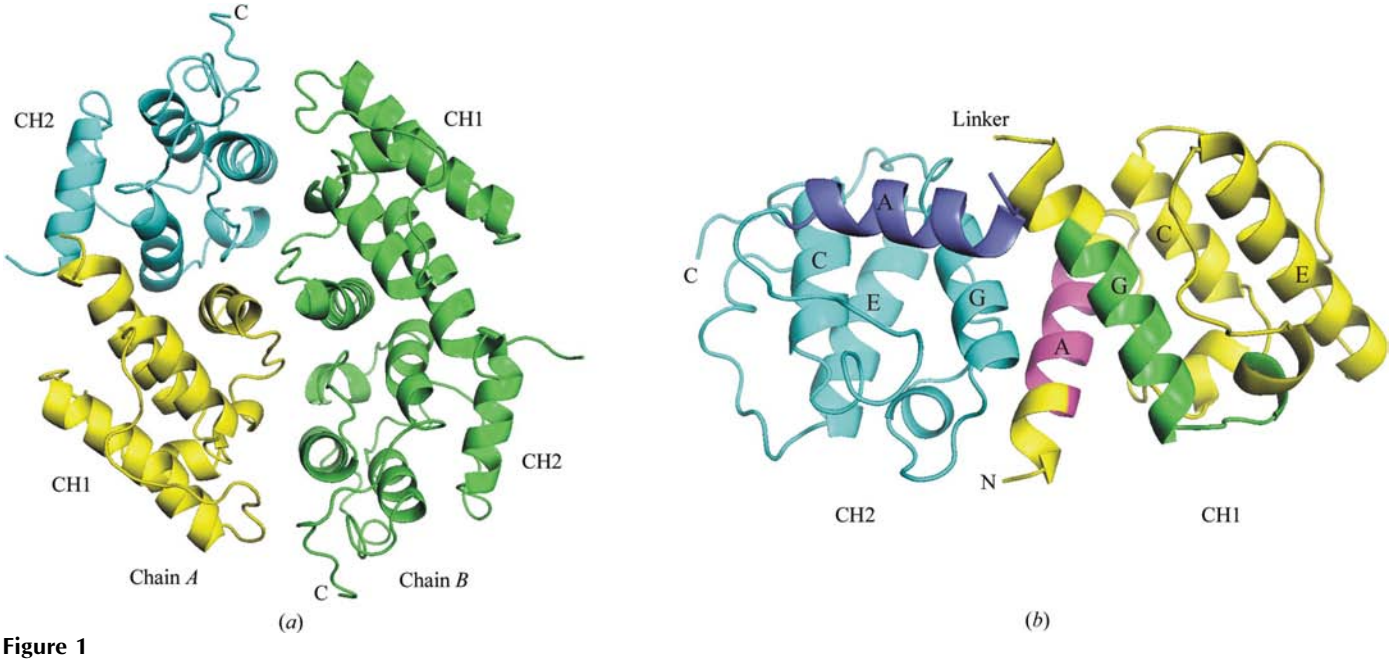


**Figure 1**
(*a*) A ribbon diagram of the asymmetric unit of FLNa ABD. There are two ABDs in the asymmetric unit. CH1 of chain *A* is shown in yellow and CH2 in cyan. Chain *B* is represented in green and the CH domains and chains are named. (*b*) A cartoon representation of FLNa ABD chain *A* in which CH domains, the linker region and the termini are marked. ABS1 is shown in magenta, ABS2 in green and ABS3 in blue and the four dominant helices are named according to previous publications.

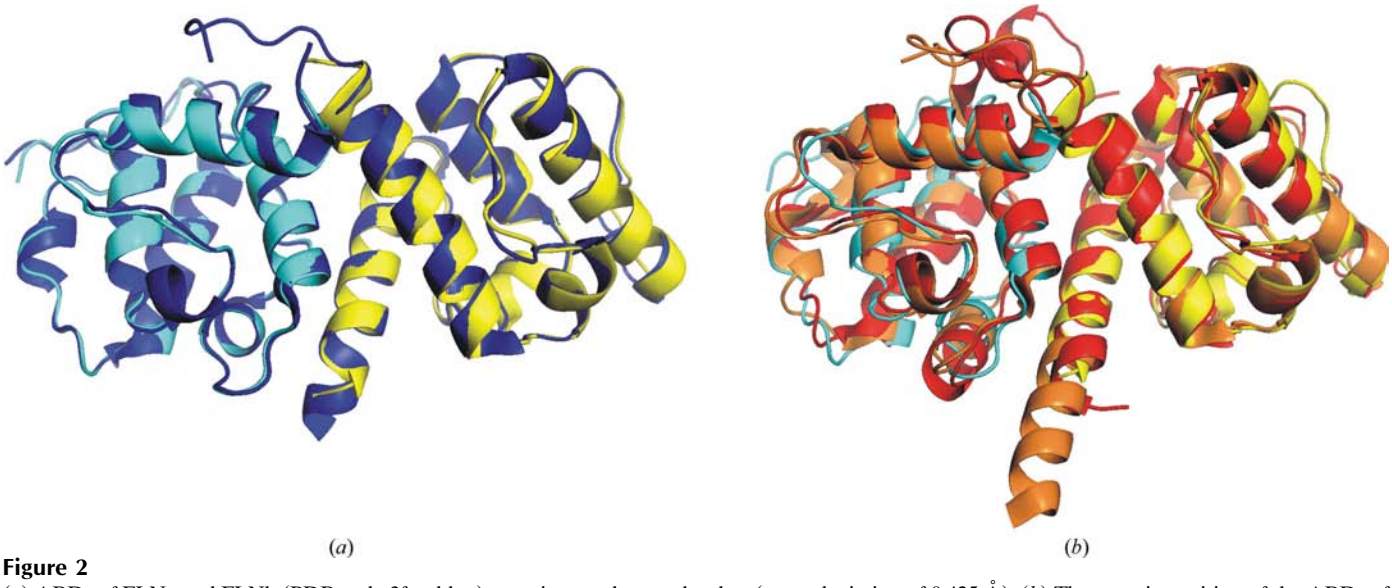


**Figure 2**
(*a*) ABDs of FLNa and FLNb (PDB code 3fer; blue) superimposed on each other (r.m.s. deviation of 0.425 Å). (*b*) The superimposition of the ABDs of human plectin (PDB code 1mb8; orange), human α-actinin 1 (PDB code 2eyi; red) and FLNa reveals that helices are highly conserved between ABDs.

an r.m.s. deviation of 0.425 Å for 211 $C^{\alpha}$ atoms (Fig. 2*a*). The sequence identity of these FLN isoforms is 88%. Other previous ABD structures with closed conformation resembled FLNa ABD much less. The most similar is the structure of human plectin ABD (PDB code 1mb8; Garcia-Alvarez *et al.*, 2003), with a sequence similarity of 36% and an r.m.s. deviation of 1.171 Å (191 $C^{\alpha}$ atoms). The structure of $\alpha$-actinin 1 ABD (PDB code 2eyi; Borrego-Diaz *et al.*, 2006) that was used as the search model has a sequence identity of 36%, but the r.m.s. deviation increases to 1.432 Å (196 $C^{\alpha}$ atoms; Fig. 2*b*). To conclude, FLNa ABD is also structurally relatively conserved compared with previous structures of ABDs. A typical ABD contains three actin-binding sites (ABSs), two of which are mapped in CH1 (ABS1 and ABS2) and one in CH2 (ABS3) (Broderick & Winder, 2005). ABS2 and ABS3 form a continuous actin-binding surface in all ABD structures, whereas ABS1 is largely buried between the CH domains (Borrego-Diaz *et al.*, 2006). Based on the ABD sequence alignments, the ABSs in FLNa ABD are composed of residues 46–55 (ABS1), 130–149 (ABS2) and 173–192 (ABS3), and they are located similarly as in other ABDs (Fig. 1*b*).

### 3.3. Patient mutations in FLNA ABD

Defects in the FLNa gene have been reported to cause serious malformations in the brain, bones and cardiovascular system, which are mostly caused by disturbance of neuronal migration during morphogenesis (Feng & Walsh, 2004). PVNH is a genetic condition that is characterized by nodules of neurons in an improper location, cardiovascular malformations and epilepsy. PVNH is often caused by loss-of-function mutations of FLNa, including deletions, insertions and nonsense mutations (Fox *et al.*, 1998; Parrini *et al.*, 2006). Some of the truncation mutations are situated in CH2 of the ABD (Q182X, R226X and Q230X). Four point mutations causing PVNH are found in CH1 (Fig. 3*a*). Two of these (A82V and M102V) change partially surface-exposed residues at the distal part of CH1 facing away from the mapped ABSs. The A128V mutation may change the protein surface close to the ABS2 and the S149P mutation disrupts the helix of ABS2 and possibly also affects the linker peptide between CH1 and CH2 that is not seen in our structure. Thus, we predict that the PVNH mutations A128V and S149P may have a direct effect on the actin binding of FLNa, whereas the E82V and M102V mutations have indirect effects.

Other inheritable conditions caused by defects in the FLNa gene are OPD spectrum disorders, which include the four related diseases OPD1, OPD2, frontometaphyseal dysplasia (FMD) and Melnick–Needles syndrome (Verloes *et al.*, 2000). The symptoms of these conditions are diverse and include skeletal malformations, cardiac defects, hernias and cleft palates. All FLNa mutations causing OPD spectrum disorders are missense mutations or small deletions conserving the reading frame (Robertson, 2007). Consistently with this, OPD patients produce full-length FLNa protein with a normal ability to bind actin cytoskeleton (Robertson, 2007). All of the OPD1- and OPD2-causing mutations and two of the FMD-causing mutations have been found in the CH2 region of the ABD (Robertson *et al.*, 2003, 2006; Hidalgo-Bravo *et al.*, 2005). They do not concentrate in any particular area but are spread over CH2 and include both exposed and embedded amino-acid residues (Fig. 3*b*). Gln170 is in the exposed surface of ABS3 and its mutation to Pro may disrupt helix *A* of CH2, which contains ABS3. Leu172 is a buried residue in the same helix and its mutation to the more bulky Phe may have a local effect that changes ABS3. Glu245 is surface-exposed close to ABS1 and its mutation to Arg may have an effect on actin binding. Other OPD mutations may have local effects at the distal part of CH2 (R196W, A200S, D203Y, P207L and A273P) or at the interface between CH1 and CH2 (D253E). This is consistent with the finding that OPD mutant proteins are produced as full-length proteins that largely retain their association with actin fibres (Robertson, 2007).

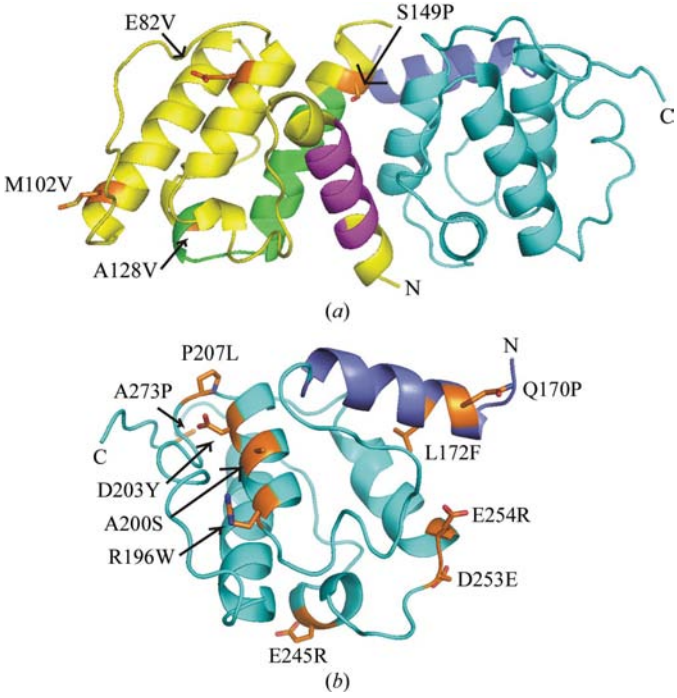


**Figure 3**
(*a*) The residues harbouring missense mutations causing periventricular nodular heterotopia (PVNH) are shown in an orange stick representation in the FLNa ABD ribbon diagram (Parrini *et al.*, 2006). All of these mutations are concentrated in CH1 of the ABD. (*b*) The OPD spectrum disorder-causing mutations are situated in the CH2 portion of the ABD (Robertson *et al.*, 2003, 2006; Hidalgo-Bravo *et al.*, 2005); the view is from the opposite direction to that in (*a*). Two of the mutations (Q170P and L172F) are located in the ABS1 region.

The authors thank Dr Martyn Winn for help in defining the weighting term used in the final refinement and for useful discussions. We acknowledge the European Synchrotron Radiation Facility for providing synchrotron radiation and we would like to thank Dr Carlo Petosa for his assistance in using beamline ID14-2. We gratefully acknowledge the Academy of Finland (Grant 114713 to JY) and the Sigrid Jusélius Foundation (Helsinki, Finland) for funding. SR is supported by the

Finnish Graduate School in Informational and Structural Biology.

## References

Borrego-Diaz, E., Kerff, F., Lee, S. H., Ferron, F., Li, Y. & Dominguez, R. (2006). *J. Struct. Biol.* **155**, 230–238.
Broderick, M. J. & Winder, S. J. (2005). *Adv. Protein Chem.* **70**, 203–246.
Emsley, P. & Cowtan, K. (2004). *Acta Cryst.* D**60**, 2126–2132.
Feng, Y. & Walsh, C. A. (2004). *Nature Cell Biol.* **6**, 1034–1038.
Flier, A. van der & Sonnenberg, A. (2001). *Biochim. Biophys. Acta*, **1538**, 99–117.
Fox, J. W., Lamperti, E. D., Eksioglu, Y. Z., Hong, S. E., Feng, Y., Graham, D. A., Scheffer, I. E., Dobyns, W. B., Hirsch, B. A., Radtke, R. A., Berkovic, S. F., Huttenlocher, P. R. & Walsh, C. A. (1998). *Neuron*, **21**, 1315–1325.
Garcia-Alvarez, B., Bobkov, A., Sonnenberg, A. & de Pereda, J. M. (2003). *Structure*, **11**, 615–625.
Gimona, M., Djinovic Carugo, K., Kranewitter, W. J. & Winder, S. J. (2002). *FEBS Lett.* **513**, 98–106.
Hidalgo-Bravo, A., Pompa-Mera, E. N., Kofman-Alfaro, S., Gonzalez-Bonilla, C. R. & Zenteno, J. C. (2005). *Am. J. Med. Genet.* **136**, 190–193.
Kabsch, W. (1993). *J. Appl. Cryst.* **26**, 795–800.
Matthews, B. W. (1968). *J. Mol. Biol.* **33**, 491–497.
Murshudov, G. N., Vagin, A. A. & Dodson, E. J. (1997). *Acta Cryst.* D**53**, 240–255.
Parrini, E. *et al.* (2006). *Brain*, **129**, 1892–1906.
Robertson, S. P. (2007). *Eur. J. Hum. Genet.* **15**, 3–9.
Robertson, S. P. *et al.* (2003). *Nature Genet.* **33**, 487–491.
Robertson, S. P. *et al.* (2006). *Am. J. Med. Genet.* **140**, 1726–1736.
Storoni, L. C., McCoy, A. J. & Read, R. J. (2004). *Acta Cryst.* D**60**, 432–438.
Tickle, I. J. (2007). *Acta Cryst.* D**63**, 1274–1281.
Verloes, A., Lesenfants, S., Barr, M., Grange, D. K., Journel, H., Lombet, J., Mortier, G. & Roeder, E. (2000). *Am. J. Med. Genet.* **90**, 407–422.